Revista Brasileira de Geofísica
RBGf
Brazilian Journal of Geophysics

Revista Brasileira de Geofísica (2007) 25(3): 321-336

ISSN 0102-261X
www.scielo.br/rbg

CRS SEISMIC DATA IMAGING SYSTEM: A CASE STUDY FOR BASIN REEVALUATION

Lourenildo Williame Barbosa Leite[1], Björn Zeno Heilmann[2] and Anderson Batista Gomes[3]

Recebido em 12 setembro, 2006 / Aceito em 27 setembro, 2007
Received on September 12, 2006 / Accepted on September 27, 2007

ABSTRACT. This paper summarizes practical results of a consistent attention to the seismic processing and interpretation of some land data lines from a set of the Tacutu graben (Brazil), where was applied the fundamental steps of the WIT imaging system grounded on the data-driven CRS (Common Reflection Surface) stack. As a major result, we expect to establish a work-flow for seismic reevaluation of sedimentary basins. Founded on the recovered wave front attributes of the CRS stack, a smooth macro-velocity model was obtained via tomographic inversion. Using this macro-model, pre- and post-stack depth migration was carried out. Besides that, other CRS-stack based processing techniques were performed in parallel as residual static correction and limited-aperture migration based on estimated projected Fresnel zone. A geological interpretation was attempted on the stacked and migrated sections. From visual details of the panels, we could interpret discontinuities, thinning, a principal faulted anticline where plays of horsts, grabens and rollovers are present. Also, part of the selected line needs more detailed processing to make better evident any present structures in the subsurface.

Keywords: CRS stack, residual static correction, seismic tomography, migration.

RESUMO. Este trabalho apresenta resultados práticos de uma atenção sistemática dada ao processamento e à interpretação sísmica de algumas linhas terrestres do conjunto de dados do gráben do Tacutu (Brasil), sobre os quais foram aplicadas etapas fundamentais do sistema WIT de imageamento do empilhamento CRS (Superfície de Reflexão Comum) vinculado a dados. Como resultado, esperamos estabelecer um fluxograma para a reavaliação sísmica de bacias sedimentares. Fundamentado nos atributos de frente de onda resultantes do empilhamento CRS, um macro-modelo suave de velocidades foi obtido através de inversão tomográfica. Usando este macro-modelo, foi realizado uma migração à profundidade pré- e pós-empilhamento. Além disso, outras técnicas baseadas no empilhamento CRS foram realizadas em paralelo como correção estática residual e migração de abertura-limitada baseada na zona de Fresnel projetada. Uma interpretação geológica sobre as seções empilhadas e migradas foi esboçada. A partir dos detalhes visuais dos painéis é possível interpretar desconformidades, afinamentos, um anticlinal principal falhado com conjuntos de horstes e grábens. Também, uma parte da linha selecionada precisa de processamento mais detalhado para evidenciar melhor qualquer estrutura presente na subsuperfície.

Palavras-chave: Empilhamento CRS, processamento sísmico, imageamento sísmico, reavaliação de bacias.

[1]Faculdade de Geofísica (UFPA), Campus Universitário do Guamá, Instituto de Geociências – 66075-110 Belém, PA, Brazil. Phone: +55 (91) 3201-7473; Fax: (91) 3201-7609 – E-mail: lwbleite@ufpa.br

[2]Geophysikalishes Institut, Universität Fridericiana Karlsruhe, Hertzstrasse, 16, Zip Code 76187, Karlsruhe, Germany. Phone: +49-721-608-4978; Fax: +49-721-71173 – E-mail: zeno.heilmann@gpi.uka.de

[3]Programa de Pós-graduação em Geofísica (UFPA), Campus Universitário do Guamá, Instituto de Geociências – 66075-110 Belém, PA, Brazil. Phone: +55 (91) 3201-7473; Fax: (91) 3201-7609 – E-mail: agomes@ufpa.br

INTRODUCTION

Obtaining a sufficiently accurate image, either in time or in depth domain, is often a difficult task in regions governed by complex geological structures and/or complicated near surface conditions. Under such circumstances, where simple model assumptions may fail, it is of particular importance to extract as much information as possible directly from the measured data. Fortunately, the ongoing increase in available computing power makes data-driven approaches feasible which, therefore, have increasingly gained in relevance during the last years.

Mann (2001) described the Common Reflection Surface (CRS) stack is a promising data-driven method, and many other contributions on CRS could be listed. It is an improved zero-offset (ZO) simulation, where its advantage over conventional methods is that for every ZO sample several kinematic wavefield attributes are obtained as useful by-products of the data-driven stacking process. As has been shown, these attributes can be applied to improve the stack itself and to support subsequent processing steps as described by Hubral (1999). Using the CRS attributes, an advanced data-processing workflow can be established leading from time to depth domain, covering a broad range of seismic reflection imaging issues in a consistent manner. The major steps of this workflow are displayed in Figure 1.

This workflow was initially applied to a dataset of the Rhein graben area aiming to obtain a structural image of relevant structures for a projected geothermal power plant. Complementary to this standard processing, the main steps of the CRS-stack based seismic imaging workflow were carried out with results that showed to be clearly superior in terms of continuity of reflection events, and signal-to-noise ratio.

A fundamental point for good visual CRS-stack results is the preprocessing of the multicoverage seismic reflection data. Preprocessing is defined as the tasks performed in several steps beginning with the geometry setup, muting of bad shot and receiver gathers, *f* filtering, *f-k* filtering, deconvolution, field static correction, and amplitude correction for displaying.

It has been reported in the recent years by several case studies of Gierse et al. (2003) that CRS stack produces reliable stack sections with high resolution and signal-to-noise ratio. The set of physically interpretable stacking parameters determined as a result of the data-driven stacking process are important because they can be used to resolve a number of dynamic and kinematic problems. The method has been extended to 3-D data, smooth and rugged survey topography, and adapted to parallel processing technology.

This paper presents results obtained for seismic land data of the Tacutu graben, aiming at basin reevaluation, where we used for reference the processing and imaging workflow described in Heilmann et al. (2004).

DATA SET

The Tacutu data set used was acquired by PETROBRAS (Tacutu Basin, Rondônia, Brazil) for petroleum exploration. The data is free for use on university research and it was obtained from ANP to support academic projects, and in this case we deal with basin reevaluation based on seismic reprocessing. The software used is non-commercial, and the research is part of the continuous cooperation between the Geophysics Department of the Federal University of Pará (Brazil) and the Wave Inversion Technology (WIT) Consortium of the University of Karlsruhe, Germany, in the spirit of Research Network. The data set is offered in the form of non-processed field records; therefore, a complete preprocessing stage was necessary, and it is partially described in the sequel.

Following the description by Eiras & Kinoshita (1990), the Tacutu basin is classified as a Mesozoic intracontinental rift, oriented NE-SW, with approximately 300 km length and 40 km width. It was developed in the central part of the Guyana shield, and it is located at the border between Brazil and Guyana. The rift is filled with sediments ranging from the Jurassic to the Quaternary, and composed of two asymmetrical half-grabens: The SW part dips southeasterly and the NE part dips northwesterly.

The structural scenario of the Tacutu basin features horsts, grabens, anticlines, synclines, flower structures, and dip inversions (rollovers). Transcurrent faulting is considered to have reactivated local features that were developed in the rift stage (see Figure 2).

The stratigraphic scenario of the Tacutu basin is divided into four depositional sequences that reflect the geological evolution of the area. The first basal sequence is represented by the volcanic Apoteri formation and by the shaly Manari formation, both related to the pre-rift phase. The second sequence is represented by the evaporitic Pirara formation, and relates to the stage of maximum stretching in the rift phase. The third sequence is represented by the sands and conglomerates of the Tacutu and Tucano formations, and it is interpreted to correspond to the continuous decrease in stretching. The fourth sequence is represented by the lateritic and alluvium of the Boa Vista and North Savannas formations.

Continuing with Eiras & Kinoshita (1990), the conclusions

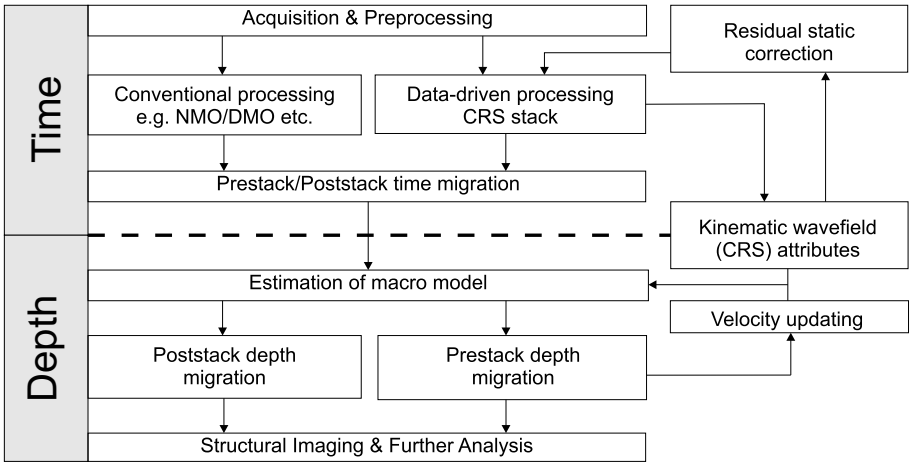

Figure 1 – Major steps of the seismic data processing in time and depth domain. Imaging procedures that can be incorporated in the CRS stack based imaging workflow.

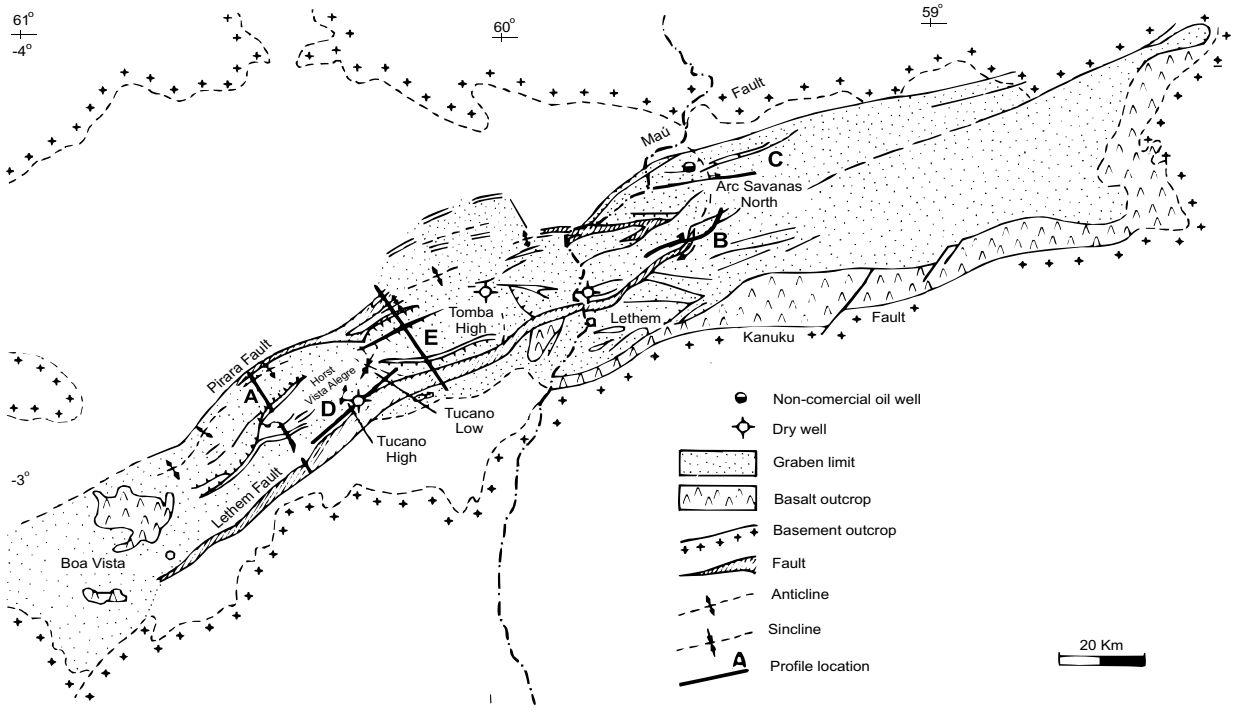

Figure 2 – Structural map of the Tacutu graben redrawn from Eiras & Kinoshita (1990) showing the direction of some seismic lines (A, D, E). The graben is about 300 km long by 40 km wide, direction NE-SW and limited by normal faults.

for the geological model of the Tacutu basin were formally based on the interpretation of the conventional processed seismic data, seismic reprocessing, seismic stratigraphy, surface geology, drilled wells, geochronology and geochemistry. Several structural styles were considered, and the most attractive were deltaic fan-shaped, compressional inversions, internal horst highs, and dip reversals. Our intention in this paper is not yet to trace new evidences for the structural scenario for the Tacutu basin, what could follow with more systematically processed data to complete at least a full block for a detail geological interpretation.

PREPROCESSING

Among the processed lines, the selected line for presentation here was limited to the one numbered 204-239, and it has the following survey information: date of acquisition 1986; direction NW-SE; length of 31.5km; 631 shot-points; 4ms of time sampling interval; 50m spacing of shotpoints and stations; charges of 0.9kg at 2m depth distributed as L-3x2/25m. The array distribution from left to right starts with a segment right-unilateral 0-48; the second part is split-spread symmetrical 48-48; the third part is split-spread asymmetrical 76-20; and the fourth part is a left-unilateral 76-0. The topography of the terrain is very smooth to almost flat.

The preprocessing steps were performed with the CWP/SU system of the Colorado School of Mines reported by Cohen & Stockwell (2000), whose data format is used in the WIT/CRS codes. The tasks consisted of 3 main parts: (1) Geometry setting; (2) Muting of bad traces; and (3) *f* and *f-k* filtering. The workflow was organized with the details kept for reference information to emphasize that the imaging process is dependent on the preprocessing steps and parameters. Other further processing and imaging involved the application of the following techniques: (4) Velocity analysis; (5) NMO stacking; (6) Migration.

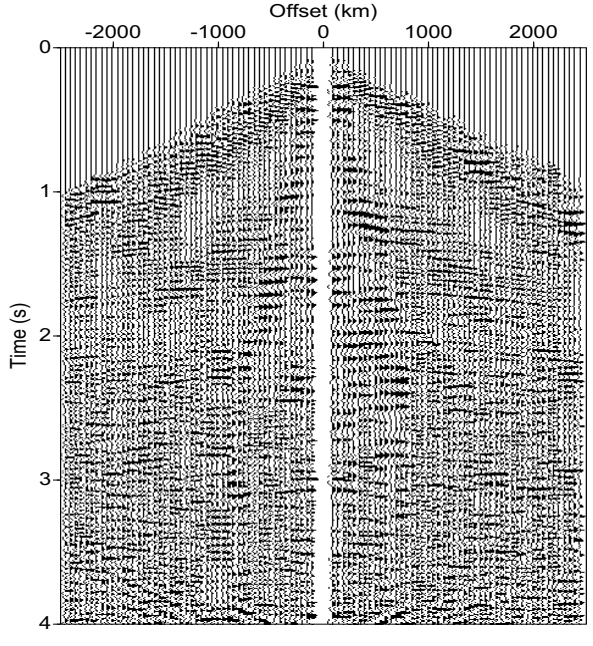

Figure 3 – Selected example of common-shot section, number 200, with *f-k* filter and dynamic gain, to show the low quality of the data characterized by the noisy aspect.

As a first observation, the original Tacutu seismic land-data (line 204-239) has many noisy sections, and for this reason several shot and receiver gathers were initially muted. Afterwards, as a result of visual analysis of all shot gathers, again several single traces had to be zeroed due to spikes and sensor wandering. As for filtering, several trapezoidal band-pass were experimented, and the decision was for adopting the case with corners 8-10-35-45 Hz. The *f-k* velocity dependent filter was used to further emphasize the cutting of surface waves and critically refracted waves. The decision for adopting the filter parameters was based on the visual analysis of the trace gathers through the spectrum and preliminary stack results, reinforcing the importance of the preprocessing stage on the CRS stack results. Also, it should be clear that, due to the flat terrain, static correction was not applied, and deconvolution were not carried out on this data to avoid further filtering. Figure 3 displays a selected example of the *f-k* filter applied to a common-shot section.

CONVENTIONAL STACK

In velocity analysis, we can single out two fundamental problems. The first one is related to the representation of the field of seismic waves, and the second is related to the criterion for expressing in quantitative form the degree of fitting between the model and the data for a certain stacking velocity. From the algorithm point of view, the velocity analysis procedure in the (x, t) domain can consists of two steps to be repeated at each point t_0 for every stacking velocity v: the normal moveout correction, and the coherency summation; both composing the velocity spectrum.

Conventionally, velocity analysis is performed on common-mid-point gathers by approximating the two-way travel time, $T(x; t_0, v)$, of primary reflection arrivals of a single interface by a second order hyperbolic model, as given by:

$$T^2(x; t_0, v) = t_0^2 + \frac{x^2}{v^2} + O(x^4). \qquad (1)$$

where x stands for the source-receiver offset, t_0 for the normal two-way travel time for $x = 0$, and v the stacking velocity. The above law is ideal for single homogeneous layer and horizontal reflector. For the next complexity of the model, we can compose an ideal medium of multiple homogeneous, isotropic, layers with horizontal interfaces and small apertures, and the above law is still of high approximation, as described in Ursin (1982). Turning to a more real Earth, the underground geology is described by a 3-dimensional variation of velocity that can be smooth or with discontinuities formed by curved interfaces, what establishes limitations on the use of the above model. For practical conventional use, we need the definition of a well-determined stacking velocity distribution, and the interval velocities can be recovered on the assumption that the stacking velocity v is approximately

equal to the root-mean-square (rms) velocity v_{rms}, as shown by Al-Chalabi (1974). As seen in the next section, the CRS stack procedure takes into account a more complex reflector geometry, but it is not so simple and direct to perform a velocity analysis at a first glance.

For the goodness of fit, numerous functionals have been proposed to be evaluated quantitatively on a given CMP gather for a certain stacking velocity, as resumed in Hubral & Krey (1980). The most common functionals measure the likeness of the NMO corrected gather's amplitude traces ($\overline{u}$) based on summation or correlation of traces, and choices of normalization. The normalized measure Semblance $S(v; t_0)$ provides NMO corrected traces, from a near first $x = x_F$ to a last $x = x_L$ offset with N_x points, and in a time window specified by some $\delta \cdot S(v; t_0)$ takes values in the interval (0,1) regardless of the signal amplitude, and it quantifies the uniformity of the signal polarity across the NMO corrected gather amplitude $\overline{u}(v; t_0)$. In the NMO stack, the function $S(v; t_0)$ can also be interpreted as the function to be optimized, from where the optimum value of the stack velocity v results.

A NMO (2-D) conventional simulated stack section is displayed in Figure 4 for qualitatively compare the development of the obtained results, where it shows the low quality of the data characterized by the noisy aspect, but we still structures can identified in the section. Figure 5 is a detail of the previous Figure 4 to show details of the clearer part of the section where structures can be identified.

CRS STACK

The CRS stack is a macro-model independent stacking method to simulate a ZO section in the (x, t) domain. The CRS stack operator is 2-dimensional, while the NMO operator is 1-dimensional. The CRS stack model is based on paraxial ray theory to obtain the traveltime formulation for a 2- and 3-dimensional inhomogeneous model with arbitrarily curved interfaces. To obtain the traveltime, two theoretical experiments are performed to generate eigenwaves: the NIP-wave and the N-wave. The first wave is associated with an exploding diffractor to produce the normal incidence point wave of radius R_{NIP} at the surface of observation. The second wave is associated with the exploding reflector to generate the normal wave of radius R_N at the surface of observation, being the exploding reflector locally approximated by a segment of an arc of circle around the NIP point. In order to satisfy the paraxial ray theory, a central ray of information has to be established, and in this case it is taken the ZO ray between the observation point and the normal incidence point (normal ray), and only primary events are taken into account. The central ray satisfies Snell's law across the interfaces, and the wavefront curvatures of the NIP-wave and N-wave change according to the refraction and transmission laws of curvature, nicely described in Hubral & Krey (1980) and used by Mann (2002).

Following Schleicher et al. (1993), the hyperbolic approximation for the two-way traveltime of primary reflections from a curved interface on a flat observation surface is given by:

$$t^2_{hyp}(x_m, h) = \left[t_0 + \frac{2\sin\beta_0(x_m - x_0)}{v_0}\right]^2 + \frac{2t_0\cos^2\beta_0}{v_0}\left[\frac{(x_m - x_0)^2}{R_N} + \frac{h^2}{R_{NIP}}\right]. \quad (2)$$

It is assumed that the velocity v_0 is known, and related to the upper layer around the observation point x_0. The independent variables x_m and h are, respectively, the midpoint and the half offset in the CMP geometry, and x_0 is the reference point of stack. The parameter β_0 corresponds to the vertical emergence angle of the wavefront at the observation point. The quantities β_0, R_{NIP} and R_N are related to the central ray in the paraxial ray theory.

The data headers contain the source, x_S, and receiver, x_G, coordinates; and the relationship to the x_m and h coordinates and are given by:

$$x_m = \frac{(x_S + x_G)}{2} \quad \text{and} \quad h = \frac{(x_S - x_G)}{2}.$$

The reference point of stack is represented by $P_0(x_0, t_0)$, and the stack trajectories are over the coordinates h and x_m.

Results of the CRS stack start with the coherence function depicted in Figure 6. This function controls the estimation of the CRS stack attributes, and Figure 7 informs the distribution of traces for the point stacks $P_0(x_0, t_0)$. It is expected that subsurface structures to be represented by definite patterns, and the better images are given by stronger patterns of continuity and higher values of coherence.

The time panels of kinematic CRS wavefield attributes, version 2D for flat observation surface, as shown in Figures 8, 9 and 10, are the following: (1) a section of the emergence angle β_0 of the ZO normal ray with respect to the normal to the measurement surface; (2) a section of the radius of curvature R_{NIP} of the wavefront relative to point source experiment at the normal incidence point (NIP) as observed at the emergence point of the normal ray; and (3) a section of the curvature R_N of the normal wavefront due to an exploding reflector element at the NIP. Coherence sections

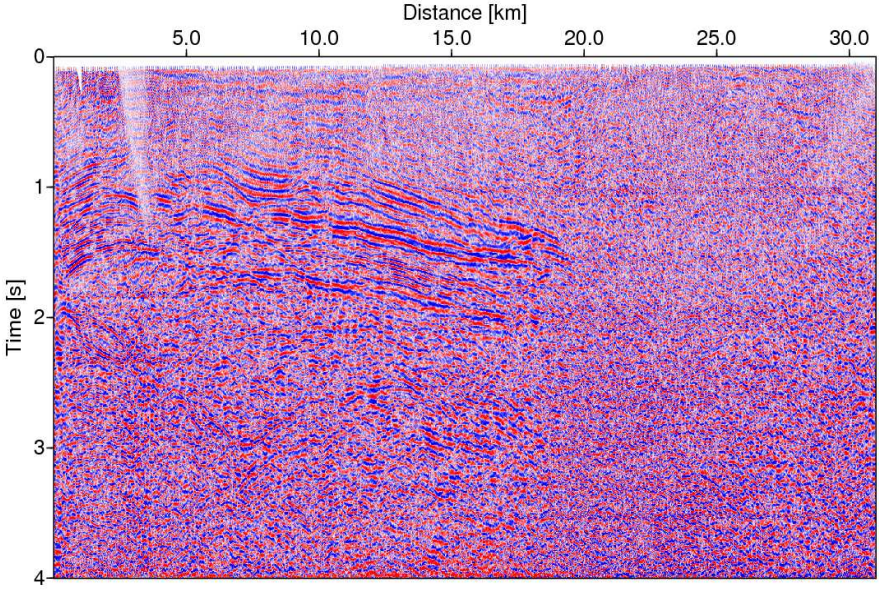

Figure 4 – Conventional 2-D stack section that shows the low quality of the data characterized by the noisy aspect, but structures can still be identified in the section.

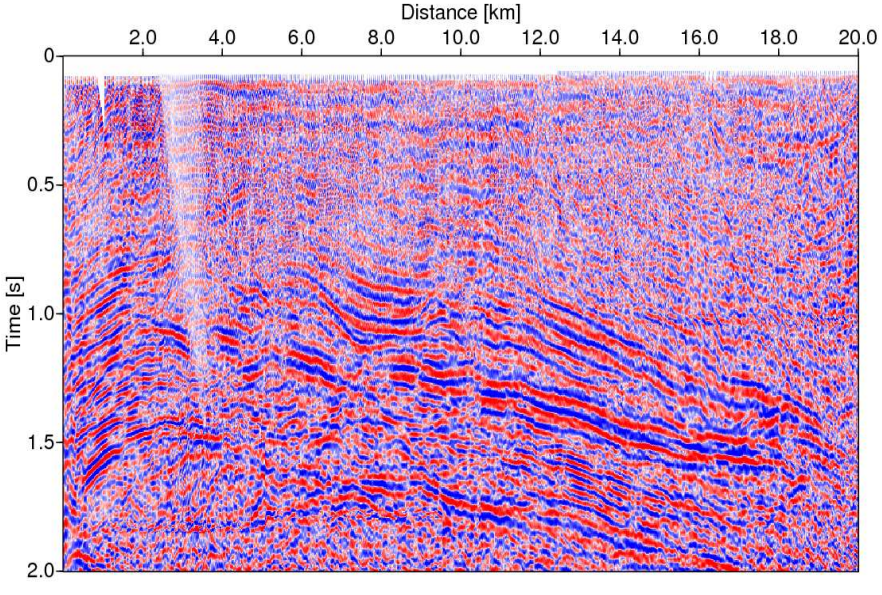

Figure 5 – Detail of the previous conventional 2-D stack limited to the window 20 km $\times$ 2s, where we can identify structures in the section.

were used to identify locations with very low coherence values, considering that such locations are not expected to be associated with reliable attributes. The sections of β_0 and R_{NIP} are used to obtain stacking velocity sections.

Figure 11 displays the basic simulated Fresnel CRS ZO panel. Common-offset gathers were also used to help analyze the difficulties in interpreting underlying reflections in the ZO sections.

RESIDUAL STATIC CORRECTION

The CRS-based residual static correction method is an iterative process close to the super-trace cross-correlation method as presented by Ronen & Claerbout (1985). In the present used approach, the cross-correlations are performed within the CRS supergathers, consisting of all moveout corrected prestack traces within the spatial stacking aperture, instead of being confined to

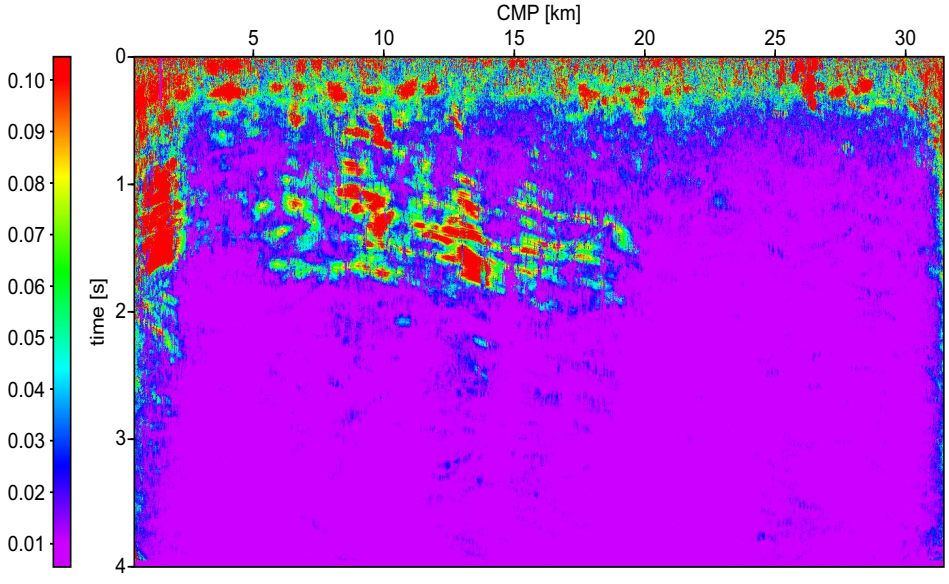

Figure 6 – Panel of coherence function for line Tacutu 204-239. Observe the low coherence pattern trends, and the best part is limited to the window 20 km $\times$ 2,0s.

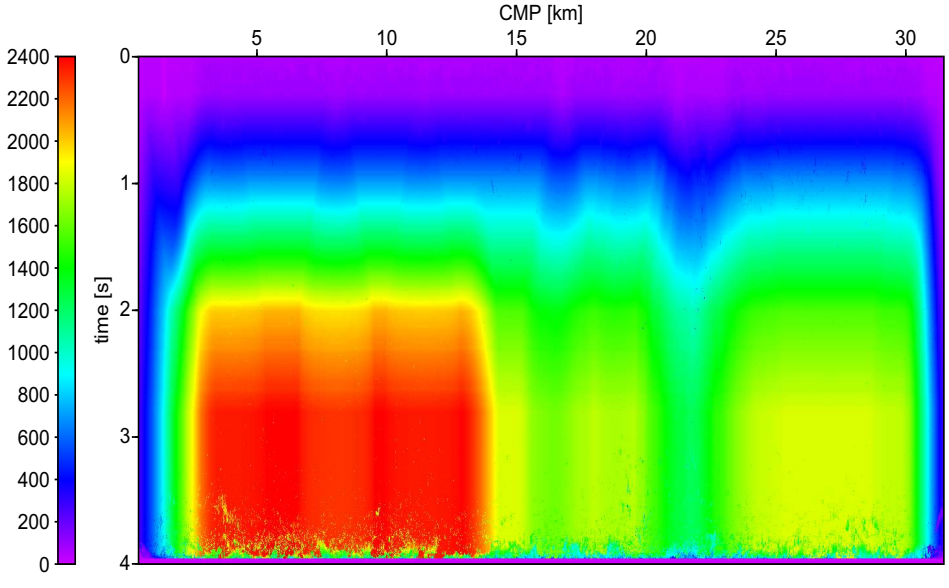

Figure 7 – Panel of density of traces that participate in the CRS stack at each point $P(x_0, t_0)$. For comparison, in a 48 $\times$ 48 traces stack window the maximum number of stacking traces would be 2304.

individual CMP, common-shot or common-receiver gathers. The moveout correction makes use of the previously obtained attributes and considers the true source and receiver elevations. Thus, elevation static correction can be omitted that may introduce non surface-consistent errors of the same scale as the searched for residual statics. Due to the spatial extent of the employed stacking operator, a supergather contains many neighboring CMP gathers. For each considered supergather, corresponding to a particular ZO location, the moveout correction will, in general, be different. Since each prestack trace is included in many different supergathers it contributes to far more cross-correlations than in methods using only individual gathers. The cross-correlations of

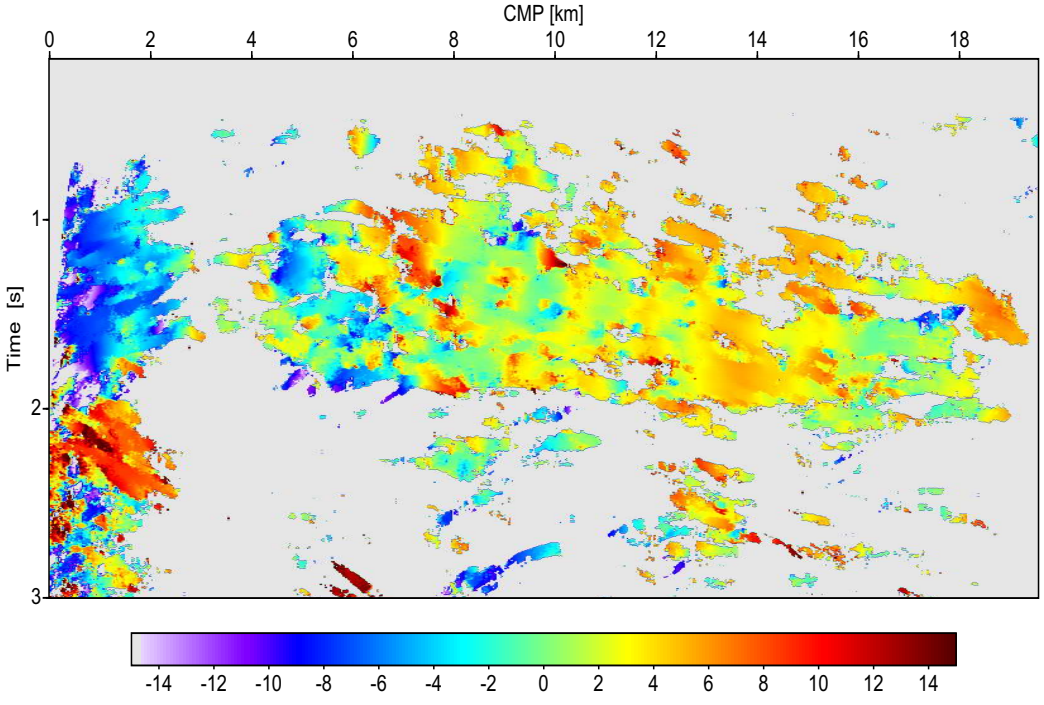

Figure 8 – Panel of emergence angle of the ZO normal ray (β_0). Observe the randon distribution of the information, and some pattern trends are limited to the window 20 km $\times$ 2,0s.

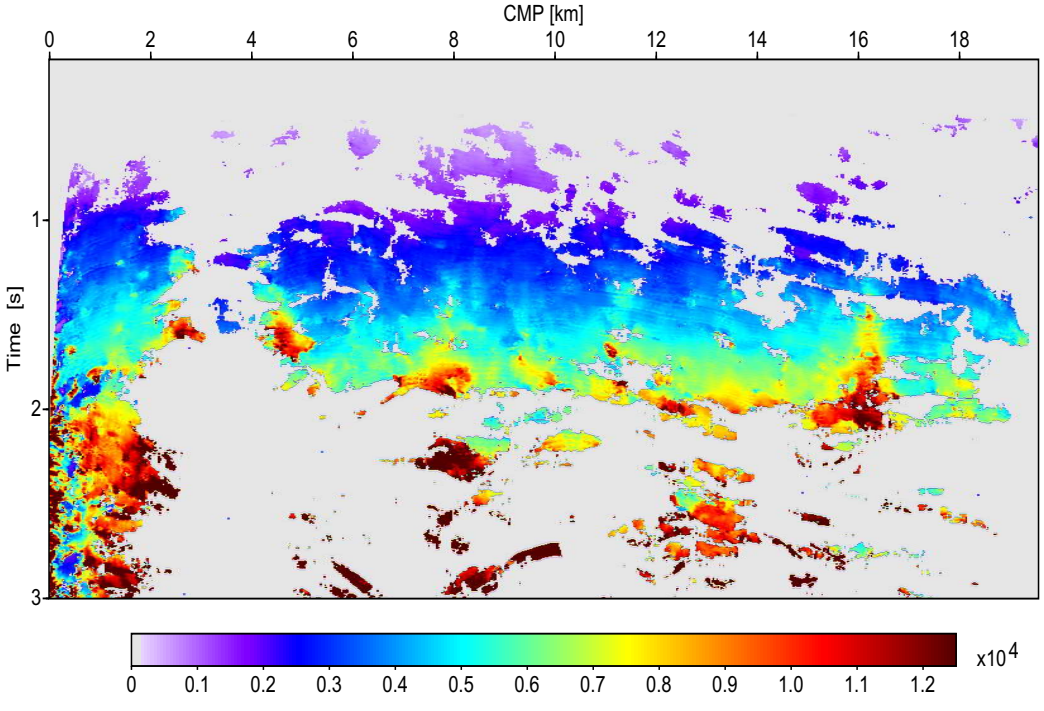

Figure 9 – Panel of radius of curvature of the Normal Incidence Point wave (R_{NIP}). Observe the low coherence in the pattern trends.

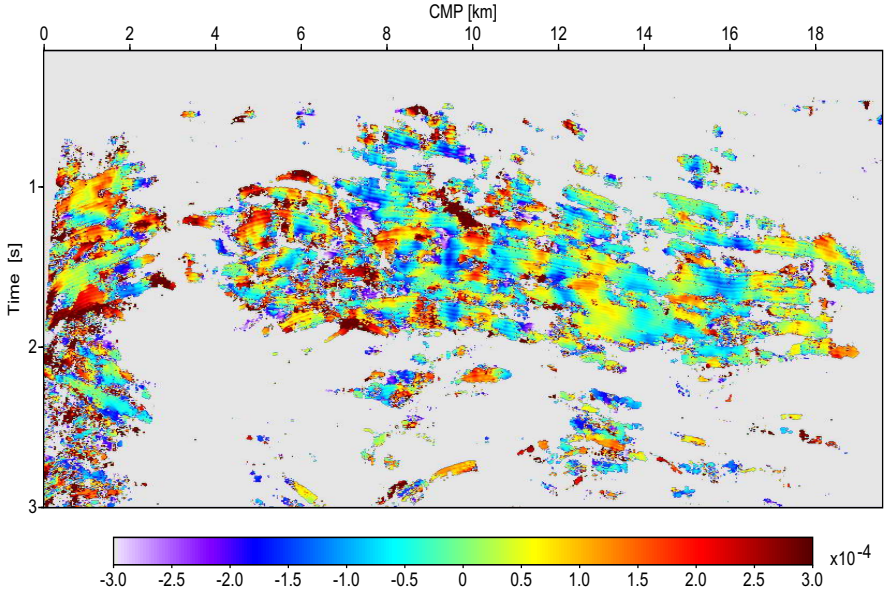

Figure 10 – Panel of curvature of the Normal wave (R_N). Observe the randon distribution of the pattern trends.

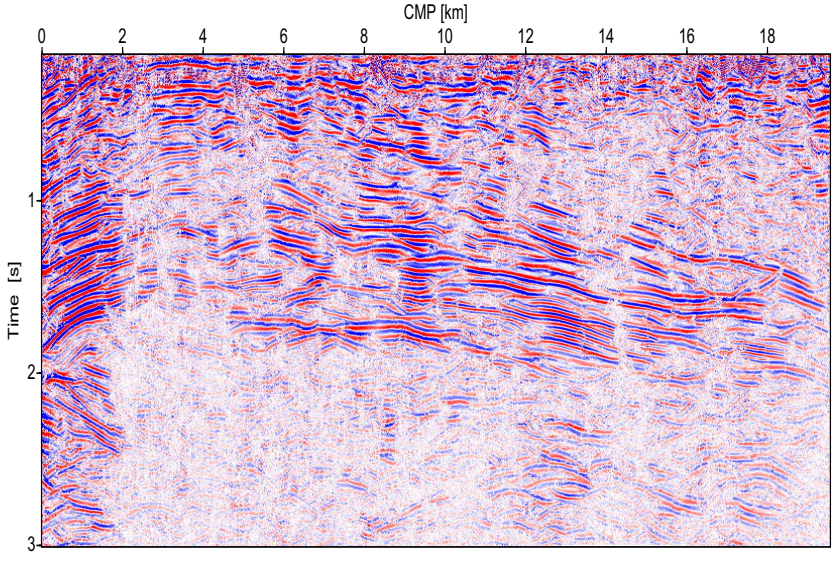

Figure 11 – ZO section simulated by CRS stack. The Fresnel window was applied, and by optimization is meant the last step in the CRS process where all the attribute are searched simultaneously.

the stacked pilot trace and the moveout corrected prestack traces are summed up for each shot and receiver location. This summation is performed for all supergathers contained in the specified target zone. The searched for residual time shifts are then expected to be associated with the maxima in the cross-correlation stacks, and they are used to correct the prestack traces. For the next iteration of residual static correction, the entire attribute search and stacking process is repeated using the corrected prestack data set.

The stack result after residual static correction and redatuming to a horizontal reference level at 90m is presented in Figure 12, and it serves for detail analysis for interpreting underlying reflectors. It can be observed that, besides an improved resolution and event continuity, also the small scale undulation of the reflection events are in great part removed. Figure 13 shows the percentage increase of coherence between optimized stack before and after residual static correction, and this further illustrates the

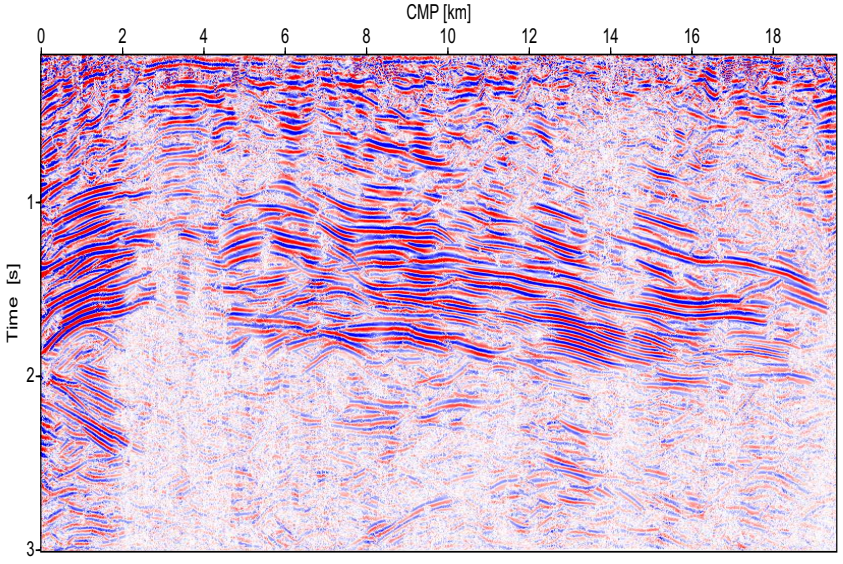

Figure 12 – Fresnel CRS optimized ZO section simulated after residual correction. This panel shows improvement with respect to the previous Figure 11.

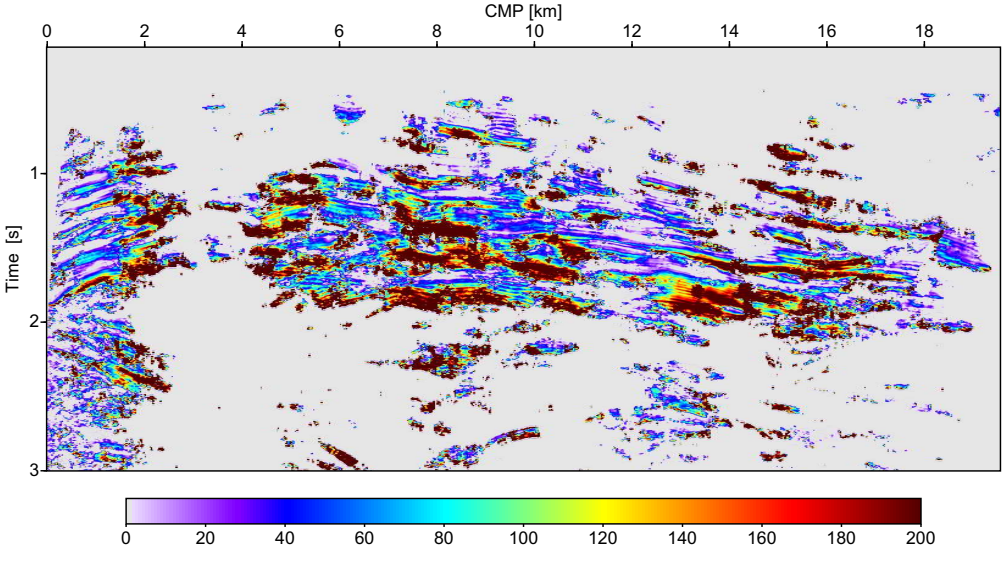

Figure 13 – Percentage of increase of coherence between optimized CRS stack measured from before and after residual static correction. Samples with low coherence values are masked out in gray, as they are not expected to be related to real reflection events.

significant improvement in coherence. Details on this approach and its application can be found in Koglin et al. (2006) and Koglin (2005).

TOMOGRAPHY

In order to obtain a depth image from the time-domain pre- and/or poststack data, it is necessary to construct a kinematical data consistent macro-velocity model. The model can be obtained from the CRS stack results by means of a tomographic inversion method based on the kinematic wavefront attributes associated with the NIP wave, as described by Duveneck (2002). As depicted in Figure 1, these attributes are the radius of curvature of the NIP wavefront and the emergence angle of the normal ray. In this method, the description of the smooth macro-velocity two-dimensional model is represented by B-splines.

In the present case study, about 1000 ZO samples, together

with the associated attribute values, were picked to achieve an appropriate resolution and reliability. Automatic picking was performed using a module based on the coherence associated with the ZO samples. The picked data was checked in order to discriminate outliers, and attributes clearly related to multiples before the tomographic inversion process was applied.

Figure 14 displays a selected window of the ZO-Fresnel CRS stack panel for detail analysis in the automatic picking for tomographic inversion, where we can see the points (green crosses) that were selected after some editing. The resulting macro-velocity model is displayed in Figure 15.

MIGRATION

The Kirchhoff time or depth migration process is expressed as an integration over the record wavefield, and for scalar wavefields in three dimensional, as described by Riede (2001) and Tygel et al. (1996), reads:

$$V(M) = -\frac{1}{2\pi}\iint_A d\xi_1 d\xi_2 W_{DS}(\vec{\xi}, M)\frac{\partial U(\vec{\xi}, t)}{\partial t}\bigg|_{t=\tau_D(\vec{\xi},M)}. \quad (3)$$

A Kirchhoff depth migration procedure based on obtained macro-velocity models from the tomographic inversion was applied to the prestack data profiles, where the necessary kinematic Green's function tables (GFTs) were calculated by means of an eikonal solver as shown by Hertweck & Jäger (2002).

The depth-migrated prestack data was muted to avoid excessive pulse stretch for shallow reflectors, and then stacked in offset direction in order to obtain the depth-migrated images displayed in Figures 16 and 18. As for an intermediate step, some common-image gathers (CIGs) are displayed in Figure 17, where muting can be seen. As most of the events in the CIGs are flat, we can state that the estimated macro-velocity model is kinematically consistent with the data. No velocity model refinement was applied after the PreSDM. Both figures show a multitude of faults and fractures, which can be traced even to larger depths. These results can be compared to results obtained by standard processing, where finite difference time migration can be applied after the NMO/DMO stack process. Although, these results show low resolution, the depth location of the reflectors should be more reliable.

As a step of the CRS-stack based imaging workflow, a poststack depth migration was performed (Figure 18). Input for the poststack depth migration are the CRS-stacked sections, and the macro-velocity models derived from the CRS attributes and tomography. Poststack depth migration can be advantageous in cases where the determination of a sufficiently accurate macro-velocity model is difficult and/or the signal-to-noise ratio is poor. In the case discussed here, where the data quality is low and the obtained macro-velocity models are not so much reliable, poststack depth migration could compete with prestack depth migration in view of resolution and image quality. In particular for the prestack depth migration (Figure 16), the faults are not as well resolved, and the shallow depth down to 750m is less imaged. Nevertheless, there are also regions, especially at greater depths, where some details are better resolved by the prestack depth migration. Therefore, poststack depth-migrated results can provide complementary information in crucial questions of geological interpretation. As an information, a preliminary Gazdag type phase-shift poststack time migration was conducted using the SU package, and used for comparison as a preliminary time migration result.

Besides, we reserved Figure 19 to this point, since it corresponds to a CRS Kirchhoff-type time migration based on the CRS attributes as a conclusive result for geometrical structure interpretation. The section shows a low quality data, but superior to the conventional methods used for reference, where structures can be identified to be more continues.

Although the CRS operator approximates better the reflection events, the approximated diffraction response might be used as alternative stacking operator to simulate a ZO section with Kirchhoff-type operators. An attractive application was proposed by Mann (2002), where the apex of the appropriate diffraction response also provides an approximation of the image location of a Kirchhoff time migration. Due to the symmetry axis, this applies to the ZO plane $h = 0$, where $\partial t_D(x_m, h = 0)/\partial x_m = 0$ yields the apex location:

$$x_{apex} = x_0 - \frac{R_{NIP} t_0 v_0 \sin\alpha}{2R_{NIP}\sin^2\alpha + t_0 v_0 \cos^2\alpha} \quad (4)$$

$$t^2_{apex} = \frac{{t_0}^3 v_0 \cos^2\alpha}{2R_{NIP}\sin^2\alpha + t_0 v_0 \cos^2\alpha} \quad (5)$$

Parametrized in terms of the apex location (x_{apex}, t_{apex}), instead of the ZO location (x_0, t_0), and with $h = 0$, the approximate ZO diffraction response reads:

$$t^2_D(x) = {t^2}_{apex} + \frac{4(x - x_{apex})^2}{v_c^2} \quad (6)$$

$$v_c^2 = \frac{2v_0^2 R_{NIP}}{2R_{NIP}\sin^2\alpha + t_0 v_0 \cos^2\alpha} \quad (7)$$

A summation along the approximate diffraction response with its result assigned to its apex approximates a Kirchhoff time migration with a constant velocity v_c, where all the attributes contribute.

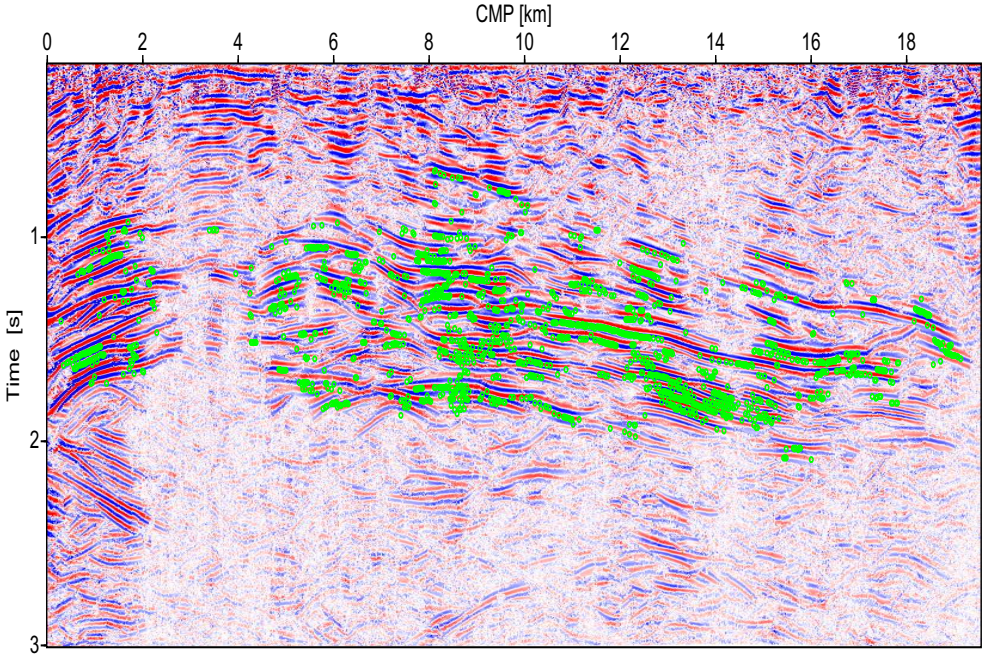

Figure 14 – Panel of locations of picked time-distance points and CRS attribute values on the ZO section (Figure 11) used for tomographic inversion.

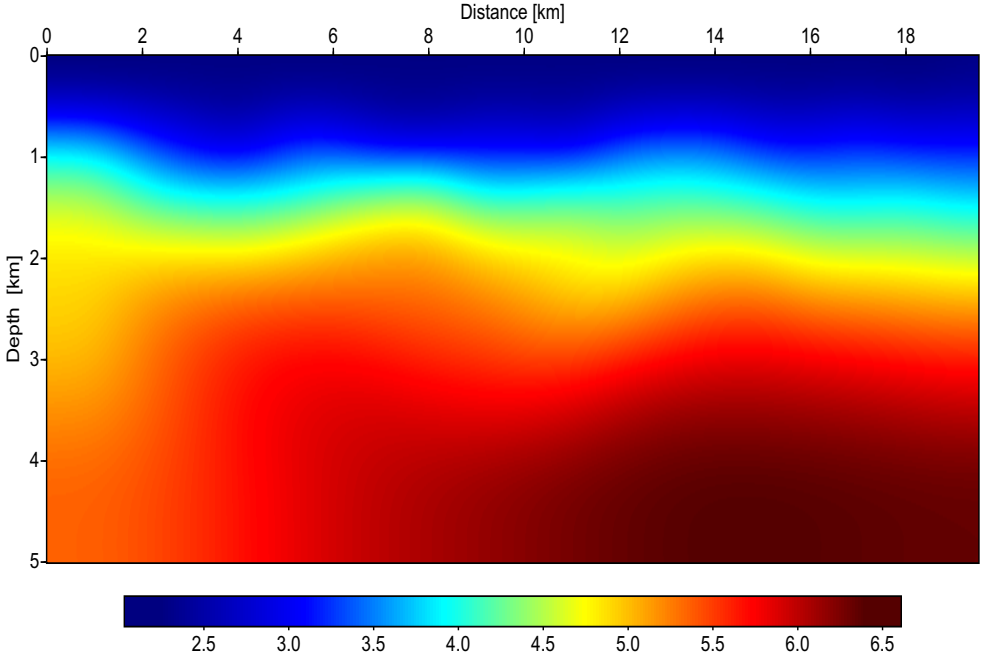

Figure 15 – Selected macro-velocity model (m/s) obtained from tomographic inversion based on the picked time-distance points and CRS attributes.

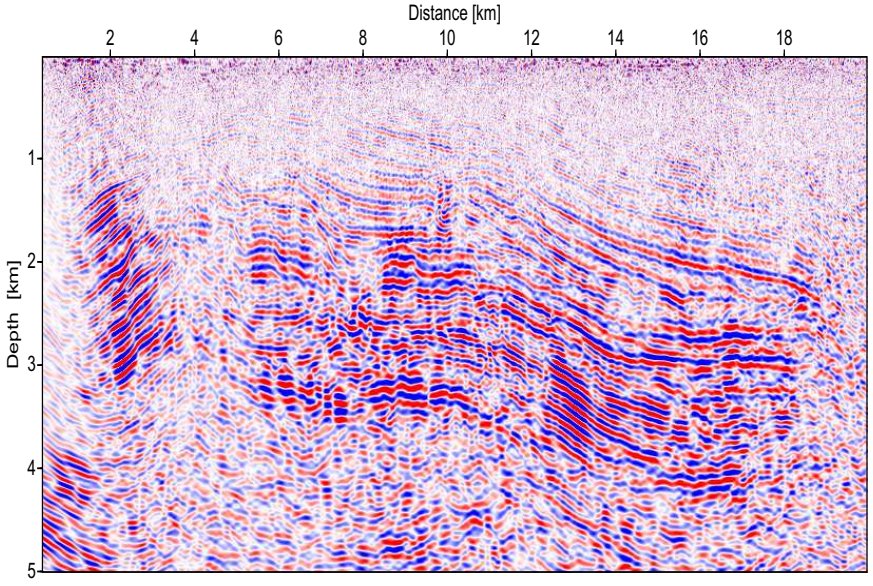

Figure 16 – Result for the preliminary Kirchhoff prestack depth migration (PreSDM) applied to the section that produced Figure 11, and based on the macro-model of Figure 15. This section shows low resolution, and it corroborates little to the geometrical interpretation of structures.

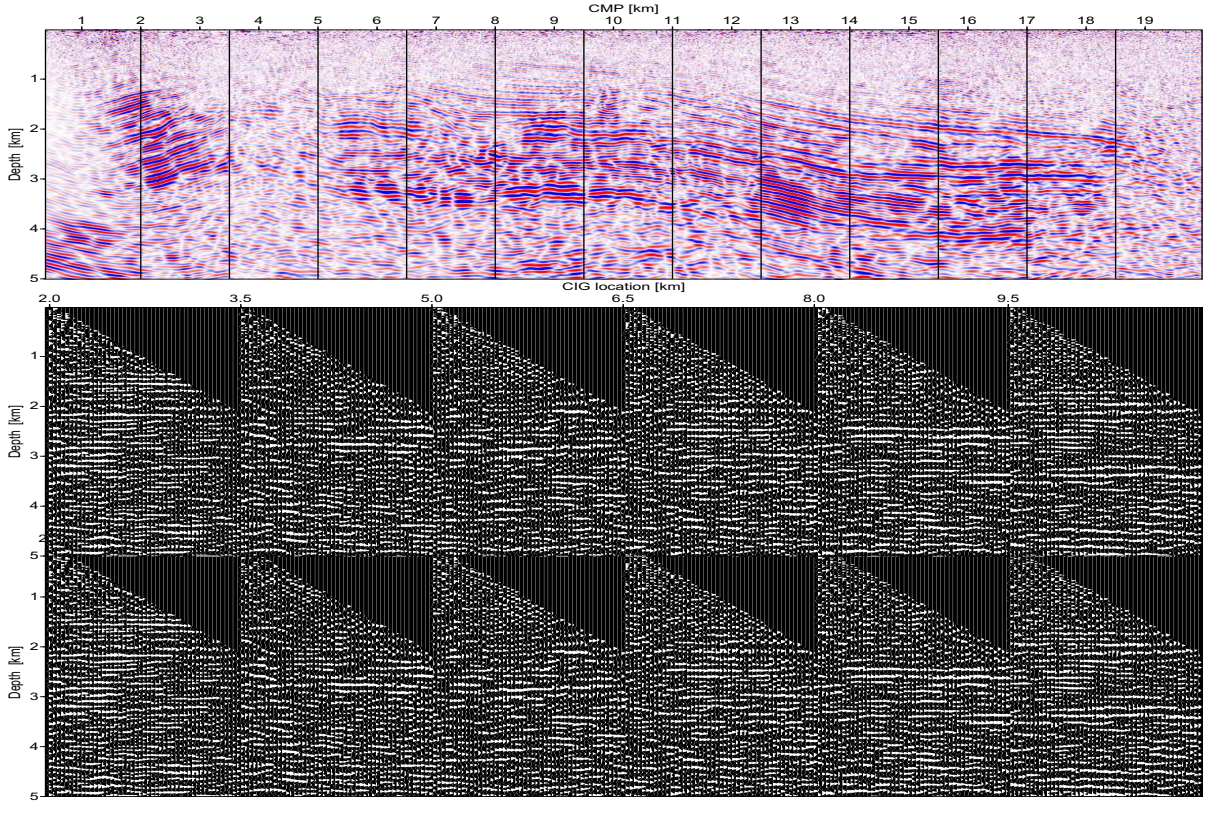

Figure 17 – Twelve common-image gathers (CIGs) extracted from the prestack depth migration result. For convenience of analysis, the PreSDM result and the respective CIG locations are also displayed.

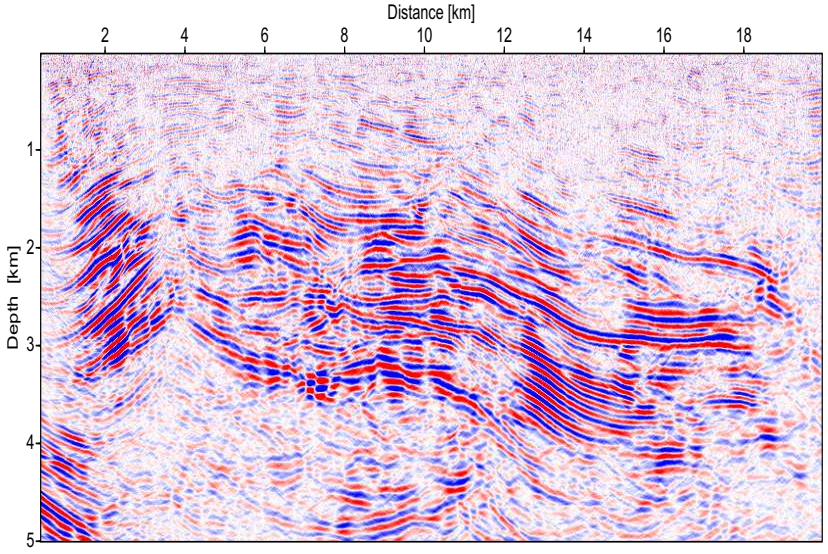

Figure 18 – Result for the preliminary Kirchhoff poststack depth migration (PostSDM) applied to section of Figure 11, and based on the macro-model of Figure 15. This section shows low resolution, but it corroborates better than the previous Figure 16 to the geometrical interpretation of structures.

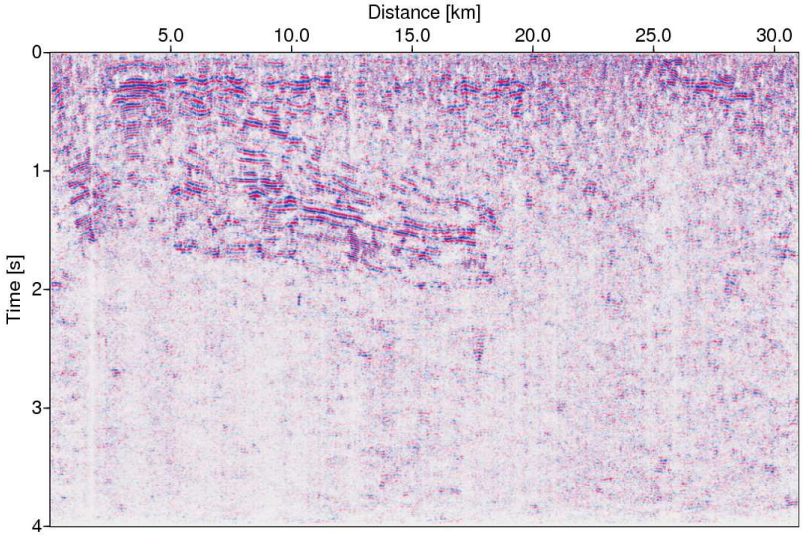

Figure 19 – CRS Kirchhoff-type time migration based on the CRS attributes. The section shows a low quality data, but superior to the conventional methods used for reference, where structures can be identified to be more continues.

In this strategy, the stack is performed along the CRS operator instead of the diffraction operator, and assigns the result to the apex (x_{apex}, t_{apex}). Figure 19 shows the result of the CRS Kirchhoff-type time migration, which is automatic and fast computed. It is obtained from the optimized zero offset section simulated by CRS stack. It is observed a scatter of points due to noise in the attributes. But, it is still observed many details like the ocean bottom line, stratification, anticlines, multiples, faults and local bodies.

CONCLUSIONS

We are limited here to some geometrical interpretation of geological structures. Considering the limitations of the coloured figures, interpretation should be carried out mainly on the basis of Figures 11, 12 and 18, being important that the maps have the proper scale, axis exaggeration and size. From screen display and details of these figures, discontinuities, thinning, a major anticline,

faults, plays of horsts and grabens, and rollovers can be indicated. On the other hand, the basement can not be easily traced. Also, the right part of the section needs more processing for structures be better evident. The referenced figures show details for drawing reflector zones related to stratigraphical units, where, e. g., a prominent reflector dips from coordinates ≈(10 km; 0.8 s) (left) to coordinates ≈(20 km; 1.5 s) (right). The most prominent anticline structure is on the left side between ≈2.0 km and ≈8.0 km horizontal distance.

The quality of the Tacutu seismic data is the main limitation in enhancing different parts for imaging the selected line. The intention is to demonstrate the applicability of the CRS-stack based imaging as a system towards basin reevaluation providing good basis for geological interpretation, and hopefully for a successful drilling.

A standard processing sequence with non commercial software was also carried out, since the present study is intended to add techniques together aiming at the imaging of geological targets present for oil exploration.

The coherence sections serve to indicate the data-driven estimated fit between the CRS stacking operators and primary reflection events in the CMP gather. But it is noticeable that the overall Tacutu seismic image quality is quite low compared to other high quality seismic image that served as reference for the present processing. Even though, the results obtained by CRS revealed good resolution as measured by signal-to-noise ratio and reflector continuity.

This example serves to reinforce our perspectives and intentions on research collaboration between different Universities, and between University and Industry to provide development and human resources for the established seismic exploration technology.

ACKNOWLEDGMENTS

The authors would like to thank the Brazilian institutions UFPA (Universidade Federal do Pará), FINEP (Financiadora de Estudos e Projetos), ANP (Agência Nacional do Petróleo, Gás Natural e Biocombustíveis) and PETROBRAS (Petróleo Brasileiro S/A) for research support, in this case the project Rede Risco Exploratório (Rede 01/03, FINEP 22.01.0763.00). The thanks are also extended to CAPES and CNPq for the scholarships of Anderson B. Gomes, to the WIT group in name of Prof. Peter Hubral, and to Prof. Milton J. Porsani for supplying the Tacutu data set. The authors would like also to thank the reviewers for the useful comments and suggestions for improving this research paper.

REFERENCES

AI-CHALABI M. 1974. An analysis of stacking RMS average and interval velocities over a horizontally layered ground. Geophysical Prospecting, 22(03): 458–475.

COHEN JK & STOCKWELL JK. 2000. Seismic Un*x Release 34: A Free Package for Seismic Research and Processing. Center for Wave Phenomena, Colorado School of Mines. Geophysical Journal International, 125: 431–442.

DUVENECK E. 2002. Tomographic velocity model inversion with CRS attributes: Annual WIT Report, p. 92–106.

EIRAS JF & KINOSHITA EM. 1990. Geologia e perspectivas petrolíferas da Bacia do Tacutu. In: GABAGLIA GPR & MILANI EJ. (Coord.). Origem e Evolução das Bacias Sedimentares. Rio de Janeiro: PETROBRAS. p. 197–220.

GIERSE G, PRUESSMANN J, LAGGIARD E, BOENNEMANN E & MEYER H. 2003. Improved imaging of 3D marine seismic data from offshore Costa Rica with CRS processing. First Break, 21(12): 45–49.

HEILMANN Z, MANN J, DUVENECK E & HERTWECK T. 2004. CRS-stack-based seismic reflection imaging: a real data example. Extended Abstracts, 66th EAGE Conference and Exhibition, Paris, France. Session P211. 4 pp.

HERTWECK T & JÄGER C. 2002. Short note: various aspects of Kirchhoff migration: Annual WIT Report, p. 133–142.

HUBRAL P. 1999. Macro-model independent seismic reflection imaging (special issue). Journal of Applied Geophysics, 42(3, 4): 137–138.

HUBRAL P & KREY T. 1980. Interval Velocities from Seismic Reflection Time Measurements. Published by the Society of Exploration Geophysicists. 203 pp.

KOGLIN I. 2005. Estimation of Residual Static Time Shifts by Means of the CRS-based Residual Static Correction Approach. Ph.D. thesis, Institute of Geophysics, University of Karlsruhe, Germany. 149 pp.

KOGLIN I, MANN J & HEILMANN Z. 2006. CRS-stack-based residual static correction. Geophysical Prospecting, 54: 697–707.

MANN J. 2001. Common-Reflection-Surface Stack: User's Manual to Version 4.2. Geophysical Institute, University of Karlsruhe, Germany. 23 pp.

MANN J. 2002. Extensions and applications of the common-reflection-surface stack method. Ph.D. thesis, Institute of Geophysics, University of Karlsruhe, Germany. 165 pp.

RIEDE M. 2001. Kirchhoff migration, demigration and seismic modeling by demigration. Ph.D. thesis, Institute of Geophysics, University of Karlsruhe, Germany. 97 pp.

RONEN J & CLAERBOUT JF. 1985. Surface-consistent residual statics estimation by stack-power maximization. Geophysics, 50(12): 2759–2767.

SCHLEICHER J, TYGEL M & HUBRAL P. 1993. Parabolic and hyperbolic paraxial two-point traveltimes in 3D media. Geophysical Prospecting, 41(4): 495–514.

TYGEL M, SCHLEICHER J & HUBRAL P. 1996. A unified approach to 3-D seismic reflection imaging, part II: Theory. Geophysics, 61(03): 759–775.

URSIN B. 1982. Quadratic wavefront and traveltime approximations in inhomogeneous layered media with curved interfaces. Geophysics, 47(7): 1012–1021.

NOTES ABOUT THE AUTHORS

Lourenildo Williame Barbosa Leite. He is professor of the Federal University of Pará, Institute of Geosciences, Faculty of Geophysics since 1979, and member of the Graduate Course in Geophysics. He was geophysicist at PROSPEC, Aero Geophysical Surveys, Rio de Janeiro, from 1977 to 1979. He graduated from the Federal University of Pernambuco, Brazil, with a Bachelor Degree in Geology in 1968. He graduated from Saint Louis University, Missouri, USA, with a Masters Degree in Geophysics in 1973, and with a Ph.D. in Geophysics in 1983. He is involved with international research cooperation, and his present area of interest is seismological exploration methods for petroleum acting in the Cooperative Research Networks of FINEP/PETROBRAS. He is a member of the Brazilian Geophysical Society, Brazilian Geological Society, Seismological Society of America, and the Society of Exploration Geophysicists.

Björn Zeno Heilmann. He received his Masters of Geophysics from the University of Karlsruhe, Germany, in October 2002, and his Doctorate degree in Geophysics in 2007. From 2002 to 2006 he was a Research Associate at the Geophysical Institute in the Wave Inversion Technology (WIT) Consortium. Besides the practical application of a CRS-stack-based imaging workflow in several research projects, he also worked on the development of the CRS stack software focusing on the influence of rugged topography and near surface velocity variations. At present he works as a geophysicist at the Center for Advanced Studies, Research and Development in Sardinia (CRS4), Italy, since September, 2007. He is a member of the European Association of Geoscientists and Engineers, and of the Society of Exploration Geophysicists.

Anderson Batista Gomes. He obtained his Bachelor Degree in Mathematics in 2004, and his Masters Degree in Geophysics in 2006, both in the Federal University of Pará (UFPA). Presently, he is a doctor student at the Graduate Course in Geophysics of UFPA in the area of the seismic methods applied to oil and gas exploration. He is a member of the Brazilian Geophysical Society.